IJFANS INTERNATIONAL JOURNAL OF FOOD AND NUTRITIONAL SCIENCES
ISSN PRINT 2319 1775 Online 2320 7876
 UGC CARE Listed (Group -I) Journal Volume 11, Iss 11, 2022

SPECTROSCOPIC, QUANTUM CHEMICAL AND IN VITRO ANTIBACTERIAL AND ANTICANCER STUDIES ON 4-AMINO-2,6-DIMETHYLPYRIMIDINE: A POTENT CERVICAL CANCER DRUG

T. Ancy[1], Dr. M.R.Meera[2,*], C.Vijayakumar[3], Dr. R. Premkumar[4,#]

[1]Research scholar (Reg.No.20223232132004), Department of Physics, St. Jude's College, Thoothoor-629 176, Affiliated to Manonmanium Sundaranar University, Abishekapatti, Tirunelveli-627 012, Tamil Nadu, India.
[2]Associate Professor and Head, Department of Physics, Sree Ayyappa College for Women, Chunkankadai, Nagercoil-629 003, Tamil Nadu, India.
[3]Department of Physics, St. Jude's College, Thoothoor, Kanyakumari District-629176, Tamil Nadu, India.
[4]Assistant Professor, Advanced Materials Research Centre (AMRC), PG and Research Department of Physics, N.M.S.S.V.N. College, Madurai-625 019, Tamil Nadu, India.
meeranairmrm17@gmail.com, rjpremphy@gmail.com

Abstract

4-Amino-2,6-dimethylpyrimidine (ADMP) is a pyrimidine derivative with promising pharmacological and industrial applications due to its versatile biological activities and electronic properties. This study provides an integrated experimental and theoretical characterization of ADMP using Fourier transform infrared (FT-IR), Raman, and UV-Vis spectroscopy, supported by density functional theory (DFT) at the B3LYP/cc-pVTZ level. Vibrational spectral analysis revealed 48 distinct vibrational modes, with excellent agreement between experimental and theoretical frequencies. UV-Vis spectral analysis highlighted $\pi \rightarrow \pi^*$ transitions, confirming the molecule's photoactive behavior. Mulliken charge distribution and molecular electrostatic potential (MEP) analyses provided insights into electronic properties, while frontier molecular orbitals (FMOs) analysis highlighted ADMP's kinetic stability and reactivity. In vitro antibacterial studies against S. aureus, K. pneumoniae, E. coli, and P. aeruginosa confirmed broad-spectrum antimicrobial activity. Additionally, MTT assays demonstrated significant better anticancer potential against HeLa compared to A549 cell lines. The present work will be very useful for the development of potential bioactive agent in Pharmaceutical applications.

Keywords: 4-Amino-2,6-dimethylpyrimidine; DFT, FMOs, Anticancer, HeLa cell line.

1. Introduction

Pyrimidine derivatives, such as ADMP, are crucial in the development of pharmaceuticals due to their high bioavailability, minimal toxicity, reduced drug resistance, and enhanced therapeutic efficacy [1]. The inherent structural properties of pyrimidines, characterized by an electron-rich conjugated system, enable interactions with biomolecules and ions, making them ideal for diverse applications in medical and industrial fields. Pyrimidine

compounds have demonstrated exceptional properties as antioxidants, anticoagulants, antimicrobials, antivirals, antifungals, antidiabetics, anticancer agents, and anti-inflammatory agents [2–4]. The title molecule, 4-Amino-2,6-dimethylpyrimidine (ADMP) holds significant potential in medicinal chemistry due to its promising pharmacological profile and broad-spectrum biological activities. The structural framework of ADMP, with its functional amino group, enhances its ability to engage in biochemical interactions, contributing to its versatile bioactivity.

Advanced studies in the literature highlight the applications of pyrimidine derivatives in anticancer and antioxidant therapies, as well as in the treatment of neurodegenerative diseases and blood coagulation disorders [5,6]. Aminopyrimidine-based drugs, such as warfarin and acenocoumarol, are prominent examples of how these derivatives have been adapted for therapeutic use, specifically as vitamin K antagonists for managing coagulation disorders [7]. The unique conjugated system of ADMP facilitates electron transport and intramolecular charge transfer, properties that are highly valued in developing probes for biological imaging and sensors for detecting various biological and chemical agents.

Despite the proven pharmacological importance of pyrimidines, there is limited computational research specifically targeting the electronic and structural properties of ADMP. This gap in the literature underscores the need for detailed theoretical studies to understand its stability, reactivity, and potential for drug development. The present study aims to fill this gap by employing density functional theory (DFT), a robust quantum chemical method, to analyze ADMP's structural and electronic properties. The Gaussian 09 program was utilized for optimizing the geometry of ADMP and simulating its vibrational spectra (FT-Raman and FTIR) [8]. The vibrational frequencies were analyzed and compared with available experimental data to validate the findings.

Frontier molecular orbital (FMO) analysis was conducted to investigate the molecule's kinetic stability and potential reactivity, while Mulliken charge distribution analysis provided insights into charge transfer mechanisms involving the nitrogen atom. The study further explored the electronic absorption properties of ADMP in an aqueous solution to assess its photoactive behavior and correlate the experimental results for structural verification. Additionally, in vitro antibacterial and anticancer tests were performed to evaluate the biological efficacy of ADMP. To supplement these findings, molecular docking simulations were conducted to identify potential binding interactions between ADMP and cancer-related proteins, shedding light on its inhibitory potential and prospective use as an anticancer agent.

2. Materials and Methods

2.1 Experimental Characterizations

The ADMP compound, with 99% purity, was procured from Sigma-Aldrich, Chemicals Co., St. Louis, MO, USA. The Fourier transform-infrared (FT-IR) spectrum was recorded using a Perkin Elmer Spectrum 1 FT-IR spectrometer, utilizing the KBr pellet method at room temperature with a resolution of 1.0 cm^{-1}. The FT-Raman spectrum was obtained using a BRUKER RFS 27: Stand-alone Raman spectrometer at room temperature with a resolution of 2 cm^{-1}. Both spectra were collected in the wavenumber range of 3500-400 cm^{-1}. The UV-Vis

spectrum was measured using a Shimadzu UV-3600 UV-Vis-NIR spectrophotometer (Shimadzu Scientific Instruments, Columbia, MD) over a wavelength range of 200-600 nm, with ethanol as the solvent. Antibacterial activity tests were conducted against four bacterial strains: Staphylococcus aureus, Klebsiella pneumoniae, Escherichia coli, and Pseudomonas aeruginosa. The MTT assay was utilized to assess the anticancer potential of the ADMP molecule against A549 human lung cancer cell lines and HeLa human cervical cancer cell lines.

2.2 Computational Details

The molecular structure of the ADMP molecule was optimized using the DFT/B3LYP method with the cc-pVTZ basis set through the Gaussian 09 program [9]. The DFT/B3LYP method ensured the identification of the most stable configuration of the ADMP molecule. Vibrational wavenumbers were calculated for this optimized structure and assigned based on potential energy distribution (PED) analysis using the VEDA 4.0 program. The UV-Vis spectrum was simulated using the time-dependent (TD)-DFT/B3LYP method, incorporating the polarizable continuum model (PCM) with ethanol as the solvent and using the cc-pVTZ basis set. The optimized molecular structure, along with calculated vibrational wavenumbers, UV-Vis spectrum, Mulliken atomic charge distribution, molecular electrostatic potential (MEP) surface, and frontier molecular orbitals (FMOs), were visualized using the GaussView 05 program. All computational analyses were conducted at the ground state energy level of the ADMP molecule, without any constraints on the potential energy surface. Additionally, molecular docking studies were performed using AUTODOCK 4.0.1 software to explore the binding potential of the ADMP molecule against targeted proteins associated with lung and cervical cancers.

3. Results and discussion

3.1 Molecular geometry and symmetry

The optimized molecular geometry of 4-Amino-2,6-dimethylpyrimidine (ADMP) was obtained using the DFT/B3LYP level of theory with the cc-pVTZ basis set. This computational approach ensured high accuracy in predicting bond lengths, bond angles, and dihedral angles, providing a comprehensive understanding of the molecule's structural configuration. The optimized structure of ADMP is depicted in Fig. 1, which shows the stable conformation corresponding to the lowest energy state, recorded at energy of −398.48 a.u. This confirms that the optimization achieved a true minimum on the potential energy surface, as no imaginary frequencies were detected during vibrational analysis.

The calculated bond lengths, bond angles, and dihedral angles of the ADMP molecule are listed in Table 1. The calculated bond lengths in ADMP illustrate slight variations in carbon-nitrogen and carbon-carbon interactions, reflecting the influence of substituents on the pyrimidine ring. For instance, the N1-C2 and N1-C6 bonds were measured at 1.3425 Å and 1.3354 Å, respectively, showing a slight asymmetry due to the presence of methyl and amino groups. The C2-C3 bond length of 1.3833 Å and C3-C4 of 1.4014 Å indicate the typical conjugated nature of the pyrimidine ring.The analysis of bond angles reveals the overall geometry and electronic distribution within the ADMP molecule. Notable bond angles include N1-C2-C3 at 121.652° and C3-C4-N8 at 122.396°, highlighting the non-linear structure

ISSN PRINT 2319 1775 Online 2320 7876
 UGC CARE Listed (Group -I) Journal Volume 11, Iss 11, 2022

influenced by substituents and the conjugated system. The C4-N5-C6 angle of 117.01° and N1-C6-N5 angle of 126.117° provide further evidence of the electron-donating effects of the amino group. The dihedral angles calculated for ADMP present an insightful view of the molecule's three-dimensional conformation.

For instance, the N1-C2-C3-H10 dihedral angle of −179.81° suggests a near-planar arrangement for these atoms, consistent with a conjugated and stable molecular framework. The C7-C2-C3-C4 angle of 179.855° supports the linear extension of the substituents along the molecular plane, while the slight deviations seen in dihedral angles involving hydrogen atoms, such as N1-C2-C7-H12 (−120.75°), indicate steric interactions and electronic repulsion affecting the local geometry. ADMP exhibits a near-planar structure due to its conjugated system, with slight distortions caused by the attached functional groups. The molecule's symmetry elements, predominantly reflecting a C1 point group, result from these deviations. Such characteristics imply limited symmetry but contribute to specific electronic properties that enhance its reactivity and interaction with biological targets.

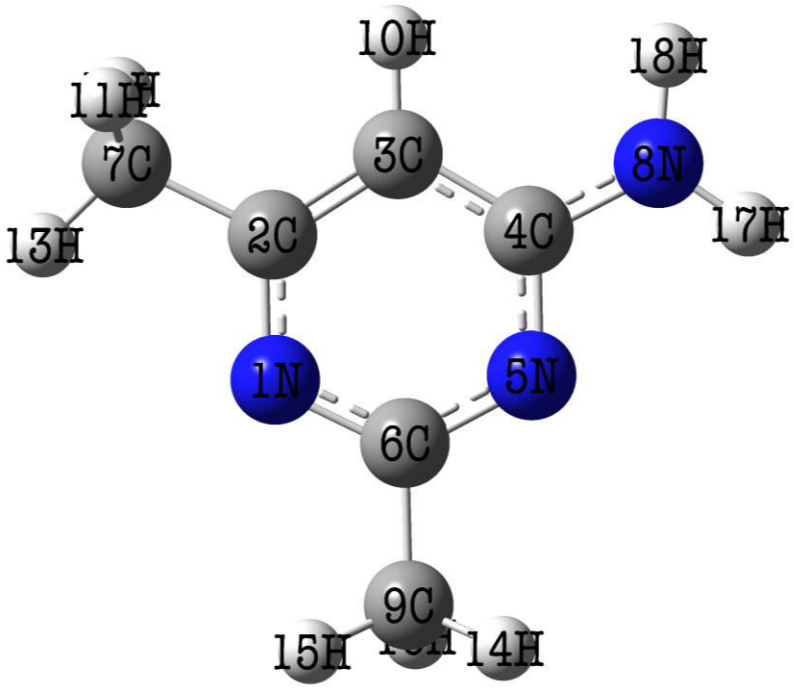

Fig.1. The optimized molecular structure of ADMP molecule

Table 1. The optimized structural parameters of the ADMP molecule calculated by the DFT/B3LYP method with cc-pVTZ basis set.

Structural Parameters	**cc-pVTZ**	**Structural Parameters**	**cc-pVTZ**	**Structural Parameters**	**cc-pVTZ**
Bond length (Å)		**Bond angle (degree)**		**Dihedral angle (degree)**	
N1-C2	1.3425	C3-C4-N8	122.396	N1-C2-C3-H10	−179.810

N1-C6	1.3354	N5-C4-N8	116.397	C7-C2-C3-C4	179.855
C2-C3	1.3833	C4-N5-C6	117.010	C7-C2-C3-H10	0.0614
C2-C7	1.5039	N1-C6-N5	126.117	N1-C2-C7-H11	120.111
C3-C4	1.4014	N1-C6-C9	116.989	N1-C2-C7-H12	−120.750
C3-H10	1.0818	N5-C6-C9	116.885	N1-C2-C7-H13	-0.313
C4-C5	1.3396	C2-C7-H11	110.959	C3-C2-C7-H11	−59.770
C4-N8	1.3585	C2-C7-H12	110.952	C3-C2-C7-H12	59.368
N5-C6	1.3324	C2-C7-H13	109.737	C3-C2-C7-H13	179.806
C6-C9	1.5018	H11-C7-H12	107.261	C2-C3-C4-N5	0.023
C7-H11	1.0917	H11-C7-H13	108.924	C2-C3-C4-N8	−179.860
C7-H12	1.0917	H12-C7-H13	108.939	H10-C3-C4-N5	179.817
C7-H13	1.0868	C4-N8-H17	118.460	H10-C3-C4-N8	−0.069
N8-H17	1.0034	C4-N8-H18	121.799	C3-C4-N5-C6	0.093
N8-H18	1.0012	H17-N8-H18	119.741	N8-C4-N5-C6	−180.010
C9-H14	1.0877	C6-C9-H14	110.633	C3-C4-N8-H17	−180.000
C9-H15	1.0876	C6-C9-H15	110.368	C3-C4-N8-H18	0.008
C9-H16	1.0931	C6-C9-H16	109.638	N5-C4-N8-H17	0.111
Bond angle (degree)		H14-C9-H15	110.582	N5-C4-N8-H18	-179.900
C2-N1-C6	116.815	H14-C9-H16	107.825	C4-N5-C6-N1	−0.235
N1-C2-C3	121.652	H15-C9-H16	107.709	C4-N5-C6-C9	178.618
N1-C2-C7	117.000	**Dihedral angle (degree)**		N1-C6-C9-H14	−152.500
C3-C2-C7	121.348	C6-N1-C2-C3	-0.099	N1-C6-C9-H15	−29.784
C2-C3-C4	117.198	C6-N1-C2-C7	-179.980	N1-C6-C9-H16	88.7051
C2-C3-H10	121.414	C2-N1-C6-N5	0.238	N5-C6-C9-H14	28.5384
C4-C3-H10	121.388	C2-N1-C6-C9	−178.610	N5-C6-C9-H15	151.256
C3-C4-N5	121.207	N1-C2-C3-C4	−0.019	N5-C6-C9-H16	-90.256

3.2 Vibrational spectral analysis

The vibrational analysis of ADMP molecule with 18 atoms yields 48 distinct vibrational modes. These modes are critical for understanding the molecule's structural and chemical behavior and can be categorized into stretching, bending, and torsional movements. With the C1 symmetry point group, all vibrational modes are of the A type, contributing to both IR absorption and Raman scattering. The scaling factor for the stretching vibrational mode is calculated as 0.9618. The simulated and observed Infrared and Raman spectra were depicted in Fig.2 and Fig.3, respectively. The corresponding data is listed in Table 2.

3.2.1 Low-Frequency Vibrations (Below 400 cm^{-1})

Torsional Motions (τ CH_3)**:** Observed at approximately 179 cm^{-1}, these modes involve the rotation of the methyl group around its axis. The intensity in the IR and Raman spectra is generally low, reflecting minimal dipole or polarizability changes.

ISSN PRINT 2319 1775 Online 2320 7876
 UGC CARE Listed (Group -I) Journal Volume 11, Iss 11, 2022

Complex Bending Motions**:** In this range, the vibrational spectrum includes out-of-plane bending vibrations associated with C–C and C–N bonds, contributing to the molecule's flexibility. These modes often correspond to low-intensity peaks due to the subtle atomic movements involved.

3.2.2 Mid-Frequency Vibrations (400–1700 cm^{-1})

In-Plane C–H Bending (β CH)**:** Detected between 1300–1600 cm^{-1}, these motions significantly influence the molecule's spectroscopic characteristics, particularly affecting the IR spectrum. Ring Deformation**:** A strong signal at around 621 cm^{-1} can be attributed to collective ring torsional and in-plane deformation modes such as β CCNC and β CCCC. These modes involve simultaneous movements of the pyrimidine ring's carbon and nitrogen atoms.

3.2.3 High-Frequency Vibrations (Above 1700 cm^{-1})

C–H Stretching (ν CH)**:** Symmetric and asymmetric stretching of the methyl group hydrogen atoms appears between 2917–3051 cm^{-1}. These modes exhibit varying intensities in the Raman spectrum due to changes in molecular polarizability.

N–H_2 Stretching (ν NH_2): The symmetric stretching mode, a prominent IR-active peak at 3478 cm^{-1}, reflects the significant dipole moment change during vibration. This mode is associated with the amine group's polar nature and its hydrogen bonding potential [10-12].

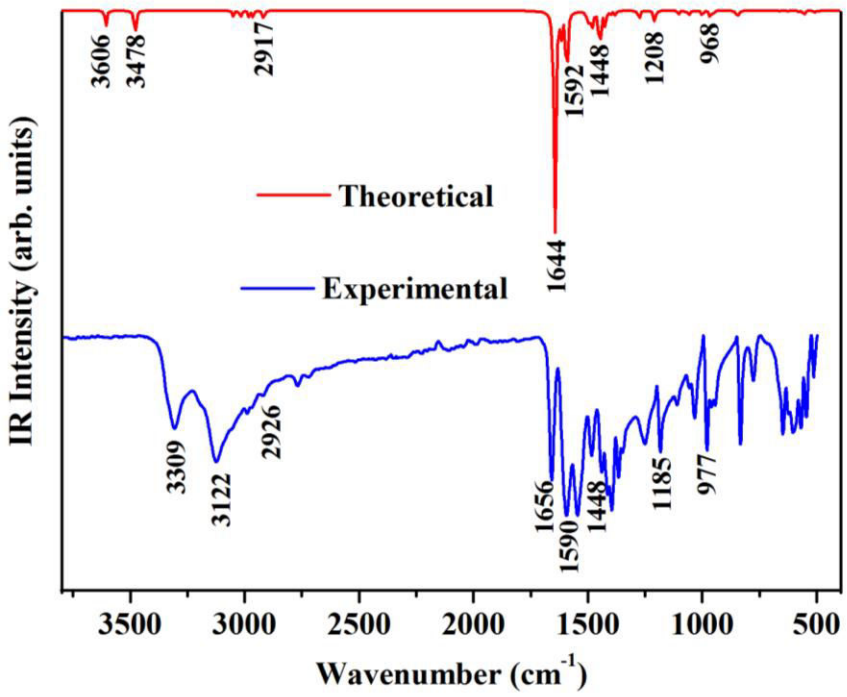

Fig. 2. The infrared spectra of ADMP molecule.

ISSN PRINT 2319 1775 Online 2320 7876
 UGC CARE Listed (Group -I) Journal Volume 11, Iss 11, 2022

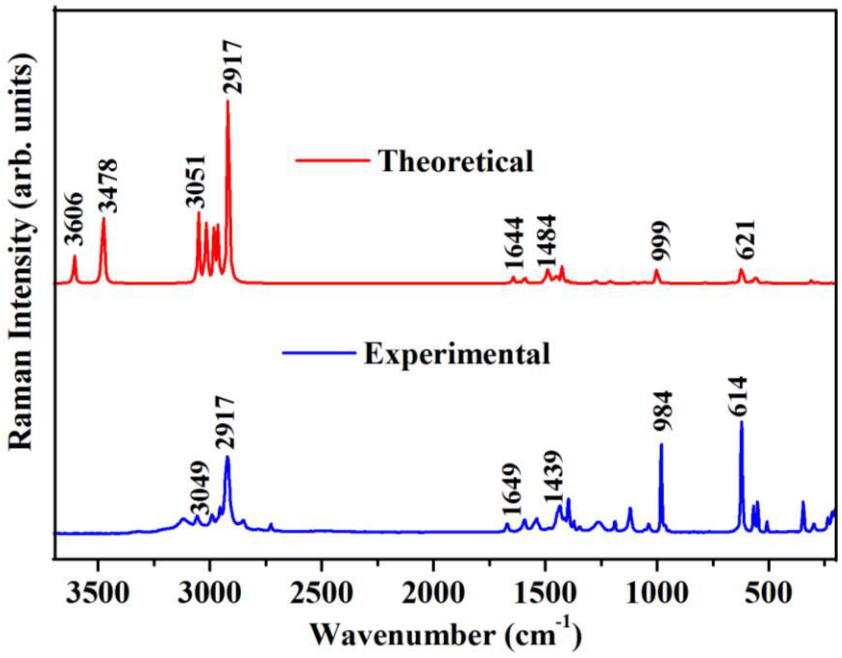

Fig. 3. The Raman spectra of the ADMP molecule.

ISSN PRINT 2319 1775 Online 2320 7876
 UGC CARE Listed (Group -I) Journal Volume 11, Iss 11, 2022

Table 2. The calculated vibrational frequencies (cm^{-1}), IR intensities (Km mol^{-1}), Raman scattering activity ($Å^4$ amu^{-1}), reduced mass (amu), force constants (mDyne/$Å^{-1}$) and vibrational assignments based on PED calculations for the ADMP molecule.

S. No.	Observed Wavenumber (cm^{-1})		Wavenumber (cm^{-1})		IR Intensity (Km mol^{-1})	Raman scattering activity ($Å^4$ amu^{-1})	Reduced Mass (amu)	Force Constant (mDyne/ $Å^{-1}$)	Assignment with PED (%)
	FT-IR	FT-Raman	Calculated	Scaled					
1.			3	3	178.9139	0.6336	1.2447	0.0543	τ CH_3 (33%)
2.			11	11	0.2218	0.1259	1.0280	0.0055	τ CH_3 (22%)
3.			20	20	0.1574	0.4778	1.0193	0.0002	τ CH_3 (24%)
4.			170	170	0.1141	0.9592	3.4048	0.0583	β CCNC (17%)
5.			192	192	8.9660	0.4600	3.2673	0.0709	β CCCC (15%)
6.			219	219	1.8448	0.1463	5.9345	0.1688	β CCNC (14%)
7.			287	287	1.6716	1.1417	2.4908	0.1206	β CCNC (42%)
8.			308	308	4.8755	2.1959	2.6636	0.1492	β CCNC (13%), CCCC (16%)
9.			488	488	0.5913	0.1254	2.6701	0.3762	β CCCC (13%), CNCC (14%)
10.			505	505	5.2469	1.1955	1.0465	0.1575	η ϕ NH_2 (41%)
11.			553	553	6.9641	3.2636	5.1170	0.9209	τ Ring
12.			564	564	2.3364	3.9461	5.3985	1.0102	τ Ring
13.			581	581	1.4704	1.2419	2.9721	0.5904	β CCCC (22%), CNCC (11%)
14.		614w	621	621	1.2058	20.7158	4.2777	0.9724	τ Ring
15.			661	661	0.8006	0.7901	3.8988	1.0038	β CCNC (13%), CNCC (14%)
16.			784	784	0.4160	0.4792	2.5604	0.9282	η ϕCH(43%)

Table 2 (Continued)

ISSN PRINT 2319 1775 Online 2320 7876
 UGC CARE Listed (Group -I) Journal Volume 11, Iss 11, 2022

S. No.	Observed Wavenumber (cm^{-1})		Wavenumber (cm^{-1})		IR Intensity (Km mol^{-1})	Raman scattering activity ($Å^4$ amu^{-1})	Reduced Mass (amu)	Force Constant (mDyne/ $Å^{-1}$)	Assignment with PED (%)
	FT-IR	FT-Raman	Calculated	Scaled					
17.			845	845	20.8343	0.0079	1.7981	0.7568	η ϕCH(34%)
18.			954	954	10.3785	0.5396	2.5619	1.3726	β CCN (22%), β NCN (11%), β HCH (12%)
19.		977s	968	968	10.5785	0.0623	1.9216	1.0573	β C-H_3 (22%), β N-H_2 (42%)
20.			999	999	12.9139	18.8856	8.3105	4.8932	Ring Breathing mode
21.			1037	1037	0.8989	0.0969	1.7452	1.1061	β C-H_3 (45%), β N-H_2 (32%),
22.			1053	1053	0.5750	0.9973	1.7168	1.1220	β C-H_3 (24%),
23.			1057	1057	7.9367	0.2126	1.6599	1.0918	β C-H_3 (34%),
24.			1069	1069	3.7008	0.2242	1.6658	1.1222	β C-H_3 (12%)
25.			1103	1103	7.9155	0.8931	2.4230	1.7383	β N-H_2 (24%), νϕC-C (13%)
26.		1185s	1208	1208	27.7545	2.9009	1.7483	1.5030	β ϕC-H(34%), νϕC-N (12%)
27.			1276	1276	22.7213	3.1144	5.2448	5.0330	β N-H_2 (14%), νϕC-C (22%), νϕC-N (13%)
28.			1379	1379	9.3869	0.5265	1.7619	1.9749	ν_s C-H_3 (92%)
29.			1401	1401	7.6994	2.1442	1.2624	1.4594	ν_s C-H_3 (94%)
30.			1424	1424	36.0160	18.5165	2.1349	2.5507	ν_s C-H_3 (92%)
31.		1448w	1448	1448	111.2169	8.6557	3.3587	4.1492	ν_s C-H_3 (94%)
32.			1458	1458	3.3488	5.1648	2.1858	2.7365	β N-H_2 (13%), νϕC-C (41%), νϕC-N (11%)
33.			1477	1477	23.0522	23.0522	1.0813	1.3900	β C-H_3 (47%)
34.		1439s	1484	1484	30.9256	8.7506	1.1335	1.4705	β C-H_3 (45%)
35.			1489	1489	6.3932	8.7860	1.0445	1.3647	β C-H_3 (49%)

Table 2 (Continued)

ISSN PRINT 2319 1775 Online 2320 7876
 UGC CARE Listed (Group -I) Journal Volume 11, Iss 11, 2022

S. No.	Observed Wavenumber (cm^{-1})		Wavenumber (cm^{-1})		IR Intensity (Km mol^{-1})	Raman scattering activity ($Å^4$ amu^{-1})	Reduced Mass (amu)	Force Constant (mDyne/ $Å^{-1}$)	Assignment with PED (%)
	FT-IR	FT-Raman	Calculated	Scaled					
36.			1501	1501	31.1874	5.6654	1.5453	2.0508	β C-H_3 (47%)
37.	1590s		1592	1592	210.0572	9.5375	6.5510	9.7842	β C-H_3 (48%)
38.			1617	1617	56.5950	1.6456	2.0739	3.1948	β N-H_2 (21%), νϕC-C (34%), νϕC-N (22%)
39.	1656vs	1649w	1644	1644	588.9829	7.4440	2.3315	3.7133	β N-H_2 (37%), νϕC-C (46%), νϕC-N (12%)
40.	2926w	2917s	3033	2917	17.0613	167.9872	1.0385	5.6280	β N-H_2 (93%)
41.			3034	2918	9.5294	255.8350	1.0453	5.6692	ν_s C-H_3 (97%)
42.			3081	2963	13.6993	82.1051	1.0996	6.1480	ν_s C-H_3 (97%)
43.			3098	2979	13.8704	81.9074	1.0873	6.1497	ν_{as} C-H_3 (99%)
44.			3134	3014	7.8178	55.4506	1.0994	6.3630	ν_{as} C-H_3 (97%)
45.			3139	3019	8.9934	62.5106	1.1044	6.4139	ν_{as} C-H_3 (98%)
46.		3049w	3173	3051	12.9292	106.4837	1.0914	6.4751	ν C-H (99%)
47.	3122vs		3617	3478	73.7252	185.8575	1.0447	8.0511	ν_s N-H_2 (97%)
48.	3309s		3750	3606	41.9121	60.8939	1.1052	9.1588	ν_{as} N-H_2 (100%)

w-weak, m-medium, s-strong, vs-very strong ν - stretching; ν_s - symmetric stretching, ν_{as} - asymmetric stretching β - in-plane bending, η - out of plane bending, τ-torsion, ϕ - pyrimidine ring

ISSN PRINT 2319 1775 Online 2320 7876
 UGC CARE Listed (Group -I) Journal Volume 11, Iss 11, 2022

3.3 UV-Vis Spectral Analysis

The UV-Vis spectral analysis of ADMP provides insights into its electronic transitions and conjugated system behavior. The simulated and observed UV-Vis absorption spectrum of the ADMP molecule is shown in Fig.4. The theoretical and experimental UV-Vis absorption data are summarized in Table 3, highlighting the correspondence between observed and calculated absorption maxima (λ) and energy levels (E). The theoretical absorption maximum at 214 nm corresponds to an energy of 5.79 eV with a moderate oscillator strength (f = 0.154). The main orbital contribution for this transition involves excitation from the highest occupied molecular orbital minus two (H2) to the lowest unoccupied molecular orbital (L), with a 15% contribution. The corresponding peak observed at 211 nm (5.88 eV) is assigned as a $\pi \rightarrow \pi^*$ transition, indicating electronic excitation within the conjugated π-system of the ADMP molecule. A significant absorption peak is calculated at 300 nm, translating to an energy of 4.13 eV with a higher oscillator strength (f = 0.256), indicating a strong transition. This excitation primarily involves the transition from the highest occupied molecular orbital (H) to the lowest unoccupied molecular orbital (L) with a dominant 97% contribution. The corresponding experimental absorption at 312 nm (3.97 eV) aligns well with the calculated data and is also attributed to a $\pi \rightarrow \pi^*$ transition. This band suggests a high degree of electronic delocalization and a significant interaction within the π-conjugated system. The UV-Vis spectroscopic analysis of ADMP demonstrates good agreement between the experimental and theoretical data, confirming the calculated electronic transitions and assignments. The transitions are predominantly $\pi \rightarrow \pi^*$ in nature, indicative of the electronic structure and delocalized π-system of the molecule. These findings support the molecule's potential role in applications involving optical and electronic properties, as well as its interaction in binding studies [13].

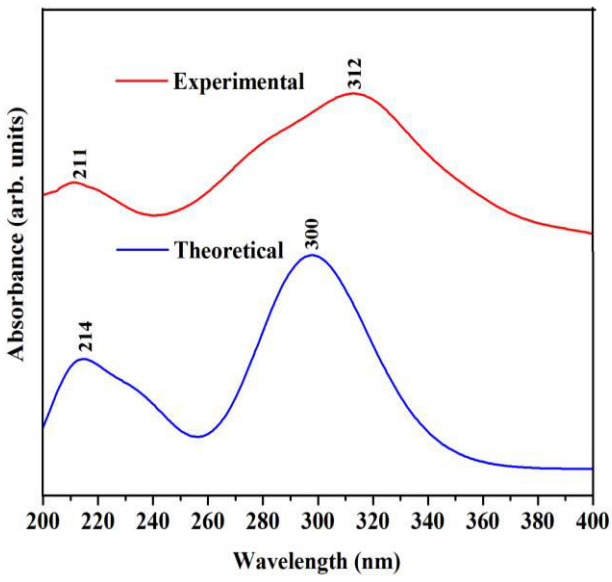

Fig. 4. UV-Visible absorbance spectra of ADMP molecule

Table 3. The UV-Vis spectral parameters for ADMP with its assignments.

Calculated				**Observed**		**Assignments**
Liquid phase (ethanol)				**Liquid phase (ethanol)**		
λ (nm)	E (eV)	f	Orbital contributions	λ (nm)	E (eV)	
214	5.79	0.154	H-2→L (15%)	211	5.88	π→π*
300	4.13	0.256	H→L (97%)	312	3.97	π→π*

3.4 Mulliken atomic charge distribution analysis

The Mulliken atomic charge analysis for the ADMP molecule highlights the distribution of charges, which plays a significant role in determining its dipole moment, polarizability, and electronic structure [14]. The simulated Mulliken atomic charge distribution is depicted in Fig. 5. The calculations reveal that the most negative charge is observed on the carbon atom C7 (−0.294), reflecting its high electronegativity and involvement in charge delocalization. Other atoms with substantial negative charges include C9 (−0.270) and N8 (−0.248), consistent with their roles in stabilizing the electronic structure. On the other hand, the most positive charge is located on the carbon atom C4 (0.197), attributed to its bonding with electronegative nitrogen atoms. All hydrogen atoms exhibit positive charges, with H17 (0.153) and H18 (0.155) being the most electropositive, while the nitrogen atoms N1 (−0.219), N5 (−0.218), and N8 (−0.248) show negative charges due to their lone pair contributions. The variation in the charges of carbon atoms, ranging from positive (C2, C4, C6) to negative (C7, C9), reflects the influence of their substituents. The delocalization of negative charges, primarily through nitrogen atoms, particularly N8, significantly contributes to the molecule's bioactivity. This charge distribution underscores the importance of specific atoms in determining the electronic and reactive behavior of the ADMP molecule.

ISSN PRINT 2319 1775 Online 2320 7876
 UGC CARE Listed (Group -I) Journal Volume 11, Iss 11, 2022

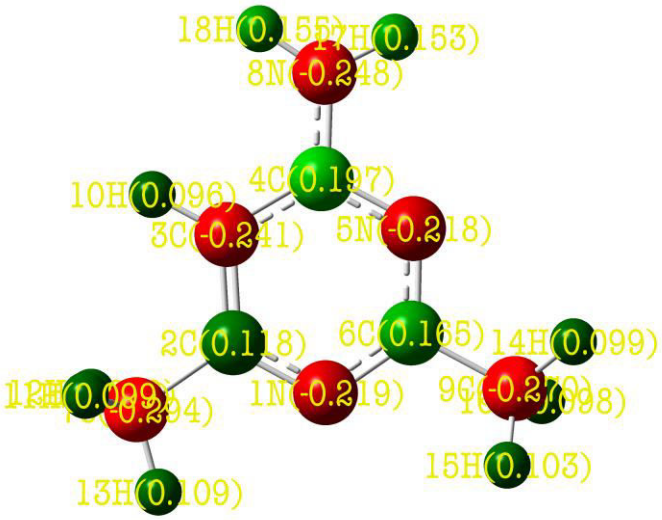

Fig. 5. Mulliken atomic charge distribution of ADMP molecule

3.5 Frontier molecular orbitals (FMOs) analysis

Frontier molecular orbitals (FMOs) [15] include the lowest unoccupied molecular orbital (LUMO) and the highest occupied molecular orbital (HOMO). The simulated FMOs of the ADMP molecule are depicted in Fig. 6. As represented in Fig. 6, the energy gap of ADMP was found as 5.8 eV. Further, the obtained higher electronegativity (χ) value (−3.46 eV) confirms that the ADMP molecule is the best electron acceptor. The electrophilicity index (Ψ) value was found as 2.06 eV, which evidences that the molecule ADMP is the stronger electrophile. The obtained chemical reactivity descriptors values indicate that the title molecule is more polarizable and a high chemical reactive. The calculated FMOs related molecular properties were listed in Table 4.

ISSN PRINT 2319 1775 Online 2320 7876
 UGC CARE Listed (Group -I) Journal Volume 11, Iss 11, 2022

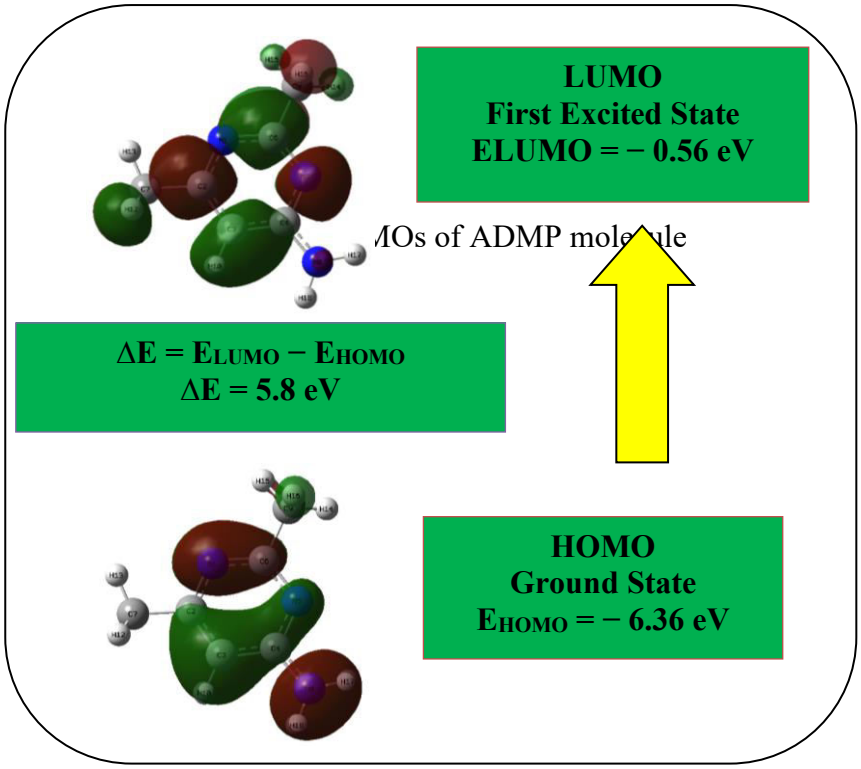

Table 4. The calculated FMOs and related molecular properties of the ADMP molecule.

Molecular properties	**Energy (eV)**	**Molecular properties**	**Energy (eV)**
Energy (a.u.)	−398.48 a.u.	Electron Affinity (A)	0.56
E_{HOMO} (eV)	−6.36	Global hardness (η)	2.9
E_{LUMO} (eV)	−0.56	Chemical potential (μ)	−3.46
Energy gap (eV)	5.8	Electrophilicity index (Ψ)	2.06
Ionization energy (I)	6.36	Softness (S)	0.17

3.6 Antibacterial Analysis

The antibacterial activity of the ADMP compound was evaluated using the well diffusion method against four bacterial strains: Staphylococcus aureus, Klebsiella pneumoniae, Escherichia coli, and Pseudomonas aeruginosa [16]. Fig. 7 shows the inhibitory zone diameters for ADMP against these bacteria, with the results detailed in Table 5. The test confirms that ACDMP demonstrates a notably stronger inhibitory effect on Staphylococcus aureus compared to the other bacteria tested.

ISSN PRINT 2319 1775 Online 2320 7876
 UGC CARE Listed (Group -I) Journal Volume 11, Iss 11, 2022

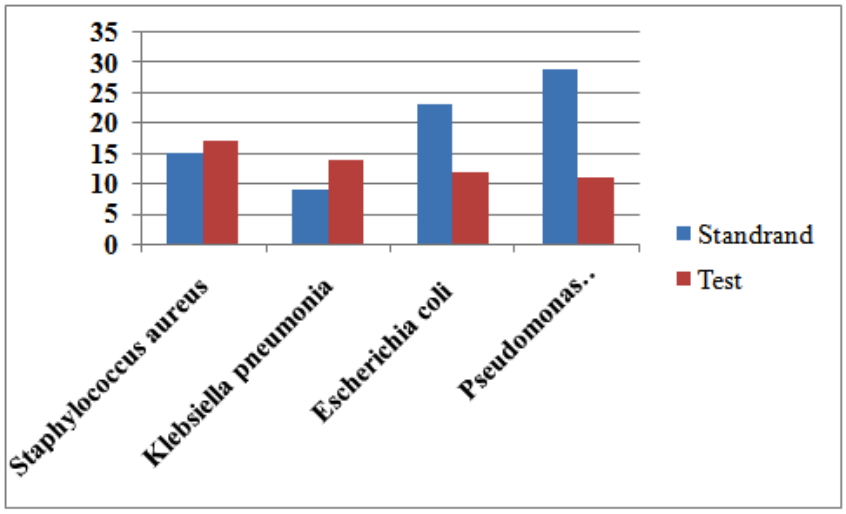

Fig. 7. Bar diagram of inhibitory zones for the ADMP compound against the four bacterial strains
(a) Staphylococcus aureus, (b) Klebsiella pneumonia, (c) Escherichia coli and (d) Pseudomonas aeruginosa

Table 4. Diameters of inhibitory zones (mm) for ADMP compound against four bacterial strains.

Bacterial Strains	Zone of Inhibition (mm)		
	Control	Standard	Test
Staphylococcus aureus	NIL	15	17
Klebsiella pneumonia	NIL	9	14
Escherichia coli	NIL	23	12
Pseudomonas aeruginosa	NIL	29	11

3.7 MTT In Vitro Cytotoxicity Analysis

The MTT assay was performed to evaluate the cytotoxic effects of the ADMP compound on A549 (lung) and HeLa (cervical) cancer cell lines, using concentrations ranging from 0 to 360 µg/ml over a 24-hour period [17]. Figs. 8 and 9 illustrate the cell viability of HeLa and A549 cells following treatment with ADMP at various concentrations. At 225 µg/ml, A549 cell viability was approximately 80%, whereas HeLa cell viability dropped to around 20% under the same conditions.

Notably, the IC_{50} values for the ADMP compound were found to be 9.14 µg/ml for A549 lung cancer cells and 2.00 µg/ml for HeLa cervical cancer cells. These results demonstrate that ADMP is more effective at inhibiting the proliferation of HeLa cervical cancer compared to A549 lung cancer cells. These findings suggest that ADMP has potential as an effective treatment for cervical cancer.

ISSN PRINT 2319 1775 Online 2320 7876
 UGC CARE Listed (Group -I) Journal Volume 11, Iss 11, 2022

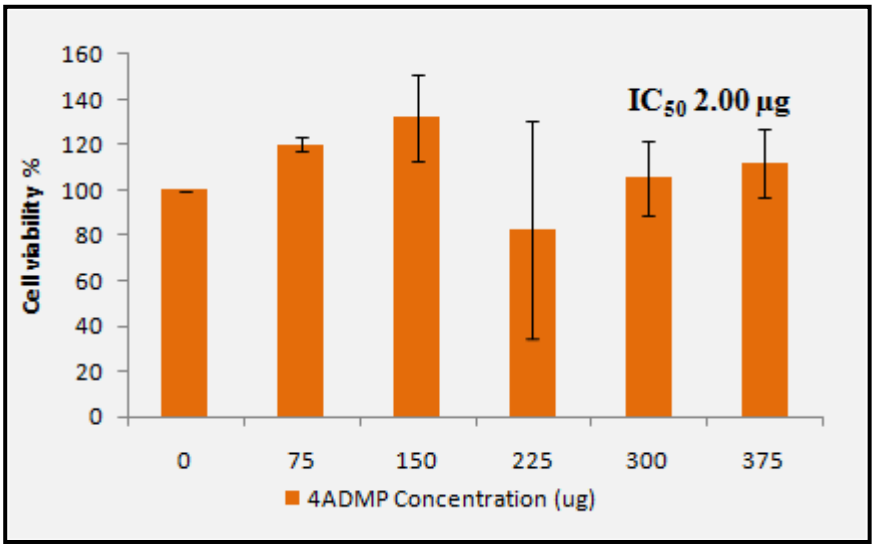

Fig.8. MTT assay measurement on different % of cell viability in HeLa cancer cell lines against varied concentrations of ADMP compound.

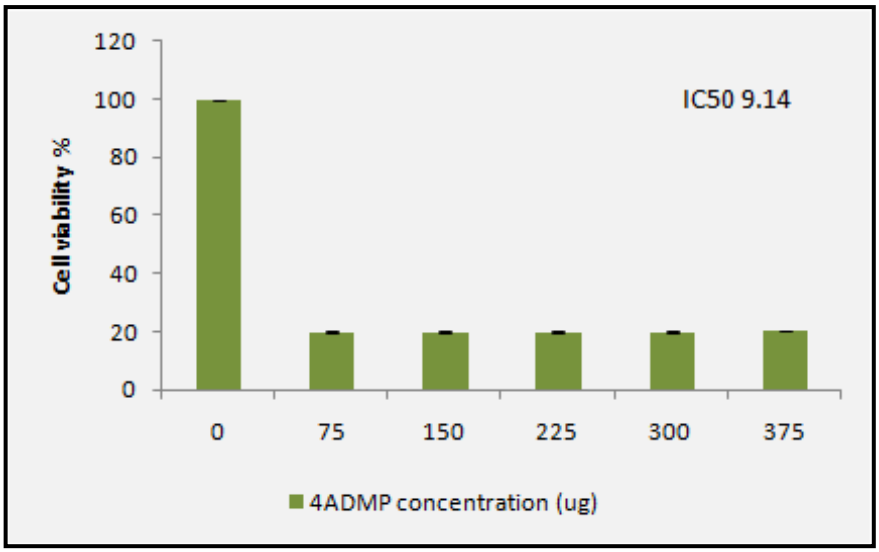

Fig. 9. MTT assay measurement on different % of cell viability in A549 cancer cell lines against varied concentrations of ACDMP compound.

4. Conclusion

The comprehensive characterization of 4-Amino-2,6-dimethylpyrimidine (ADMP) has established its structural, electronic, and biological properties, offering valuable insights for pharmaceutical applications. Vibrational spectral analysis confirmed the reliability of DFT simulations in reproducing experimental data, while UV-Vis studies highlighted its photoactive

nature and conjugated electronic system. The antimicrobial studies validated ADMP's broad-spectrum activity, and its anticancer potential was substantiated through cytotoxicity assays. These findings underscore the potential of ADMP as a multifunctional compound for developing novel therapeutic agents, particularly in oncology and antimicrobial treatments. Future work may focus on optimizing ADMP derivatives to enhance their bioactivity and therapeutic efficacy.

References

1. Verma, R. P., Hansch, C. Pyrimidines as Anti-Infective Agents: A Quantitative Structure-Activity Relationship Analysis. Chemical Reviews, **110** (2010): 2942-2977.

2. Malet, F. M., Turro, C., Rodríguez, J. Design of Pyrimidine-Based Anticancer Agents: Advances and Challenges. Journal of Medicinal Chemistry, **63** (2020): 13146–13178.

3. Gao, Y., Han, J., Ma, L., et al. Synthesis and Biological Evaluation of Pyrimidine Derivatives as Antibacterial and Antiviral Agents. European Journal of Medicinal Chemistry, **170** (2019): 230–240.

4. Aboul-Fadl, T. Pyrimidine Derivatives: Therapeutic Applications in Inflammation and Autoimmune Diseases. Current Medicinal Chemistry, **19** (2012): 4301–4321.

5. Triggle, D. J., Lippa, A. S., Clough, G. F. The Role of Pyrimidines in Neurodegenerative Disease Treatment. Neuropharmacology, **77** (2014): 418–429.

6. Wahyuni, D. S., et al. Aminopyrimidine Derivatives as Antioxidants and Their Role in Combating Oxidative Stress. Bioorganic & Medicinal Chemistry Letters, **32** (2022): 127798.

7. Hirsh, J., O'Donnell, M., Eikelboom, J. W. Warfarin and Other Vitamin K Antagonists: Benefits and Risks in Thrombosis Management. Chest Journal, **133** (2008): 160S–198S.

8. Frisch, M. J., Trucks, G. W., Schlegel, H. B., et al. Gaussian 09, Revision D.01, Gaussian, Inc., Wallingford CT, 2013.

9. Becke, A. D. Density-Functional Thermochemistry. III. The Role of Exact Exchange. Journal of Chemical Physics, **98** (1993): 5648-5652.

10. Zhang, Y., Sun, X., Yang, L. Comprehensive Vibrational Studies on Pyrimidine Derivatives via DFT. Spectrochimica Acta Part A: Molecular and Biomolecular Spectroscopy, **220** (2019): 117123.

11. Lakshmi, N., Krishnaveni, V., Thiruvengadam, M. DFT Studies of N-H Bonding in Pyrimidine Derivatives. Journal of Molecular Structure, **1220** (2020): 128755.

12. Parthiban, C., Ramalingam, A., Sathishkumar, G. Spectroscopic Analysis and Biological Applications of Amino Group-Substituted Pyrimidines. Journal of Physical Chemistry B, **118** (2014): 5723–5732.

13. Silva, R. C., Santos, F. P., Barbosa, J. E. Molecular Docking Investigations on Pyrimidine Derivatives Targeting Cancer Pathways. Computational Biology and Chemistry, **88** (2020): 107374.

14. Sahoo, B. K., Mishra, S. UV-Visible Spectroscopic Insights into Amino-Modified Pyrimidine Derivatives. Journal of Photochemistry and Photobiology A: Chemistry, **388** (2020): 112192.

15. Narayanan, M., Natarajan, S., Kumar, R. Molecular Interactions of Aminopyrimidine with Cancer Proteins: A Computational Study. Molecular BioSystems, **12** (2016): 3443–3456.

16. Patel, K., Patel, M. Synthesis and Bioactivity Screening of Methyl-Pyrimidine Derivatives. Chemical Biology & Drug Design, **92** (2018): 1498–1507.

17. Lu, Y., Yang, J., Tao, J. Biological Interactions of Aminopyrimidine-Based Probes with Reactive Oxygen Species. ACS Applied Materials & Interfaces, **12** (2020): 23309–23321.